Progress In Electromagnetics Research C, Vol. 137, 155–168, 2023

Study on the Composite Scattering Characteristics of Ship Target on the Sea Surface with Its Wake

Tian-Ci Yang, Ye Zhao*, Shao-Shuai Yu, Guo-Shan Wu, Xin-Cheng Ren, and Peng-Ju Yang

Abstract—Ship's movement on the sea surface will produce wake extending for several kilometers. In order to study the electromagnetic scattering characteristics of the composite scene of sea surface, ship, and wake, this paper combines geometric optics with physical optics (GO-PO), Kirchhoff approximation (KA) and facet scattering field model of sea surface to calculate the electromagnetic scattering characteristics of this composite scene. Firstly, the geometric model of the composite scene of sea surface and Kelvin wake is established by using Elfouhaily omnidirectional spectrum and classical ship wave generation theory. Secondly, the generated geometric overlay model of the wake and sea surface is combined with the ship to generate a composite scene model of the sea surface, ship, and wake. Finally, the scattering echoes of sea surface and wake are calculated by KA and facet scattering field model of sea surface, and the scattering echoes of ship is calculated by GO-PO. On this basis, the electromagnetic characteristics of the composite scene of sea surface, ship, and wake under different conditions are discussed. The research conclusion has certain reference value for the detection of ship and wake in complex sea conditions.

1. INTRODUCTION

In recent years, with the development of surface traffic, the research on ship targets on the sea surface has become an important research direction in the field of target detection and recognition.

In the study of ships, many researchers tend to study the synthetic aperture radar (SAR) imaging algorithm of ships. In order to solve the problem of low computational efficiency in local sliding window detection, Yao et al. [1] proposed a fast two-parameter coupled folded arm resonator (CFAR) algorithm based on fast Fourier transform. Bai et al. [2] proposed an anchor-free feature balance joint attention detector for multi-scale SAR ship detection based on key point prediction strategy. Qian et al. [3] presented a technique that utilized a particle swarm optimization algorithm to estimate Doppler parameters, with the aim of enhancing ship target imaging in a bistatic forward-looking synthetic aperture radar system. Wang et al. [4] investigated sea surface scattering and ship dynamics motion model by analyzing the geometric difference between the actual complex sea surface ship target and Geosynchronous Earth Orbit unmanned aerial vehicle bistatic SAR geometric structure. They established a composite scattering model to accurately depict sea surface motion with high confidence. Based on this model, they proposed a precise focusing imaging algorithm for moving ship targets in rough sea conditions. Zhang et al. [5] developed a robust algorithm for tracking multiple ship targets using SAR images, with small prior samples, high false alarm rate, and defocusing interference. Li et al. [6] proposed a multifeature based local saliency enhancement ship target detection method that can effectively enhance targets and suppress clutter noise under side lobes and speckle noise conditions.

Received 20 April 2023, Accepted 25 August 2023, Scheduled 4 September 2023
* Corresponding author: Ye Zhao (zhaoye07074135@163.com).
The authors are with the School of Physics and Electronic Information, Yan'an University, Yan'an 716000, China.

Some scholars have also dedicated their efforts to research beyond ship SAR imaging algorithms. Wu et al. [7] proposed a strengthened asymmetric receptive field block algorithm for the accurate detection of infrared ships. Huang et al. [8] proposed a discrete component decomposition method to solve the dynamic scene scattering problem of ships in motion on the ocean. Shi et al. [9] proposed an electromagnetic scattering method based on six degrees of freedom for time-varying ship-sea composite scenes.

In addition to studying the ships themselves, many scholars have also turned to the wake induced by ship navigation. Luo et al. [10] used the two-scale method (TSM) to calculate the backscatter coefficient distribution of ship wakes on a finite-depth sea surface. Sun et al. [11] simulated nonlinear ship waves on an infinite fluid using a numerical scheme combining the boundary integral method with the Jacobian-free Newton Craycroft method, and elucidated the influence of ship size on Kelvin ship waves. To investigate the impact of ship parameters and speckle noise in numerically simulated SAR images, Wang et al. [12] combined electromagnetic scattering models with deep learning techniques to explore nonlinear ship wake detection methods. Song et al. [13] introduced wake effects into a polarization reflection distribution model for rough seas and combined polarized skylight distribution with rough sea wake reflection distribution to establish a polarization characteristic model for rough sea wakes. They simulated the polarized reflection distribution characteristics of rough sea wakes under skylight background. Li et al. [14] proposed an automatic ship speed estimation method based on the two-dimensional Kelvin wake spectrum of SAR images. By partitioning the two-dimensional dynamic sea surface, and conducting feature selection verification, Bi et al. [15] were able to determine the location of Kelvin wake. To investigate the impact of underwater object motion on electromagnetic scattering from the sea surface, Deng et al. [16] developed a method that combines computational fluid dynamics with electromagnetic imaging. Wei et al. [17] developed a method for detecting Kelvin ship wakes in SAR by utilizing periodic structure scattering calculations.

However, many studies only pay attention to the ship itself or the wake induced by the ship, without considering their combined presence in real-world scenarios. In this paper, the combination of ship and wake induced by ship is considered, and the electromagnetic scattering characteristics of the composite scene composed of sea, ship, and wake are studied.

The rest of this paper is structured as follows. Section 2 outlines the modeling of sea surface and Kelvin wake. Section 3 describes the methods for calculating electromagnetic scattering from the sea surface and ship. Section 4 presents simulation results and discussions. Finally, Section 5 forms the conclusion.

2. ESTABLISHMENT OF THE COMPOSITE SCENE

In this paper, a two-dimensional sea spectrum is simulated by combining the Elfouhaily omnidirectional spectrum with the Longuet-Higgins directional distribution function:

$$W\left(k,\varphi\right)=W_{Elf}\left(k\right)G_{LH}\left(k,\varphi-\varphi_{w}\right)/k \tag{1}$$

where $W_{Elf}\left(k\right)$ is the Elfouhaily omnidirectional sea spectrum [18], $G_{LH}\left(k,\varphi\right)$ the Longuet-Higgins directional distribution function, k the wavenumber, φ the wave number direction angle of the sea waves, and φ_w the wind direction.

Lord Kelvin's theory provides a way to calculate the wave elevation of a ship moving at a speed U_s in the $-x$ direction. The equation is given as follows:

$$z_k(x,y)=Re\int_{-\pi/2}^{\pi/2}A(\theta)\exp[-ik_k\sec^2\theta(x\cos\theta+y\sin\theta)]d\theta \tag{2}$$

where $k_k=g/U_s^2$, g is the acceleration due to gravity, and $A(\theta)$ is the free spectrum that depicts the ship's characteristics, which can be written as follows:

$$A(\theta)=\frac{2k_k}{\pi}\sec^3\theta\int\int\frac{\partial y(x,z)}{\partial x}\exp\ \left[k_k\sec^2\theta(ix\cos\theta+z)\right]dxdz \tag{3}$$

where $y(x,z)$ is the hull equation of the ship. If we consider a simple hull shape with parabolic waterlines and if it is a wall-sided ship with draft depth d, then [19]:

$$y(x,z) = \begin{cases} b\left(1-\dfrac{x^2}{l^2}\right), & -d \le z \le 0, -l < x < l \\ 0, & z < -d \end{cases} \tag{4}$$

where $2b$ is the beam, and $2l$ is the length of the ship.

The ship parameters simulating Kelvin wake are shown in Table 1. The geometric structure of the ship is shown in Figure 1. Figure 2 simulates the geometry of the synthetic scene of sea surface and wake in different ship directions under the ship speed of 10 m/s and the wind speed of 3 m/s after considering the ship position.

Table 1. Parameters of the Kelvin wake simulation ship.

Parametric Name	Parametric Value
Ship length	184.65 m
Ship width	23.91 m
Side wall draft depth	8.00 m

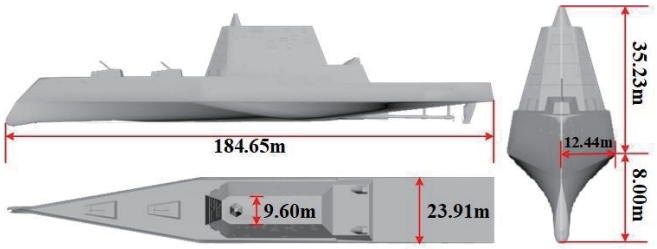

Figure 1. The geometric structure of the ship.

3. COMPOSITE SCATTERING CALCULATION METHOD

3.1. Scattering Calculation of Sea Surface

The scattering area of a two-dimensional sea surface can be categorized into two regions: the specular region and diffuse scattering area. The facet scattering field model of sea surface by capillary waves [20, 21] is used to calculate the facets that contribute significantly to the diffuse scattering region, while the Kirchhoff approximation (KA) method is used to calculate the facets that contribute significantly to the specular region scattering. As a result, the scattering field of each individual facet of the sea surface can be represented as:

$$E_{pq}\left(\hat{\mathbf{k}}_i, \hat{\mathbf{k}}_s\right) = \begin{cases} E_{pq}^{KA}(\hat{\mathbf{k}}_i, \hat{\mathbf{k}}_s), & \text{specular region} \\ E_{pq}^{facet}(\hat{\mathbf{k}}_i, \hat{\mathbf{k}}_s), & \text{non-specular region} \end{cases} \tag{5}$$

where,

$$\mathbf{E}_{pq}^{KA}(\mathbf{r}) = \frac{ik\exp(ikR)}{4\pi R}\hat{\mathbf{k}}_s \times \int \left[(\hat{\mathbf{n}} \times \mathbf{E}) - \eta\hat{\mathbf{k}}_s \times (\hat{\mathbf{n}} \times \mathbf{H})\right] \exp\ \left[-ik(\hat{\mathbf{k}}_s - \hat{\mathbf{k}}_i) \cdot \mathbf{r}'\right] dS' \tag{6}$$

$$\mathbf{E}_{pq}^{facet}\left(\hat{\mathbf{k}}_i, \hat{\mathbf{k}}_s\right) = \frac{ik^2(\varepsilon-1)\Delta S}{8\pi n_z} F_{pq} \frac{e^{ikR}}{R} e^{-i\mathbf{q}\cdot\mathbf{r}_0} \left[B(\mathbf{k}_c^+)\mathbf{I}_0(\mathbf{k}_c^+) + B(\mathbf{k}_c^-)\mathbf{I}_0(\mathbf{k}_c^-)\right] \tag{7}$$

In this equation, the following terms are used: $\hat{\mathbf{k}}_i$ represents the propagation direction vector of the incident electromagnetic wave; $\hat{\mathbf{k}}_s$ represents the propagation direction vector of the scattered

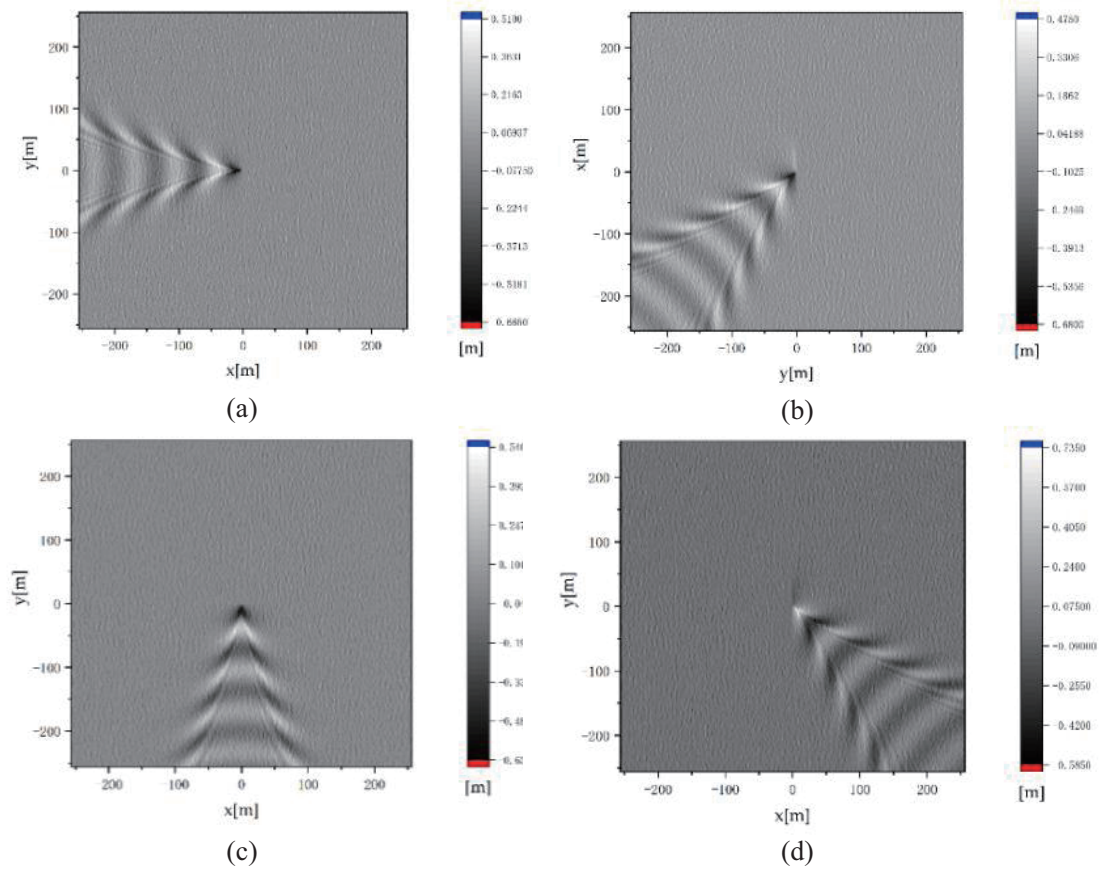

Figure 2. Geometric model of sea surface and ship Kelvin wake composite scene under different headings. (a) $\varphi_{ship} = 0°$, (b) $\varphi_{ship} = 45°$, (c) $\varphi_{ship} = 90°$, (d) $\varphi_{ship} = 135°$.

electromagnetic wave; k is the number of electromagnetic waves; $\hat{\mathbf{n}}$ represents the normal vector; η is the intrinsic impedance; R is the distance between the center of the plane element and the observation point; $\boldsymbol{E}$ and $\boldsymbol{H}$ represent the total electric field and total magnetic field on the boundary surface, respectively; ΔS is the area of the small facet on the sea surface; r_0 represents the position of the center point of the small plane element; $\mathbf{k}_c$ is the wavenumber vector of the capillary component; $B(\mathbf{k}_c)$ is the amplitude of the capillary wave; F_{pq} is the polarization factor. The specific expressions for $B(\mathbf{k}_c), \mathbf{I}_0(\mathbf{k}_c)$ and F_{pq} can be found in reference [22].

The total scattered field on the sea surface can be obtained by adding up the scattered fields of all facets present on the sea surface:

$$\mathbf{E}_{pq}^{sea}(\hat{\mathbf{k}}_i, \hat{\mathbf{k}}_s) = \sum_{m=1}^{M} \sum_{n=1}^{N} E_{pq}(\hat{\mathbf{k}}_i, \hat{\mathbf{k}}_s) \tag{8}$$

where M and N are discrete points of two-dimensional sea surface. The refined facet scattering field model (RFSFM) of the sea surface is the model defined in Equation (8).

By calculating the scattering field of all elements according to RFSFM, the scattering coefficient of a single sample of a static sea surface at any time can be obtained

$$\sigma_{pq}(\hat{\mathbf{k}}_i, \hat{\mathbf{k}}_s, t) = \lim_{R\to\infty} \frac{4\pi R^2}{A} \left[\mathbf{E}_{pq}^{sea}(\hat{\mathbf{k}}_i, \hat{\mathbf{k}}_s, t)\mathbf{E}_{pq}^{sea}(\hat{\mathbf{k}}_i, \hat{\mathbf{k}}_s, t)^*\right] \tag{9}$$

where A is the two-dimensional sea surface area irradiated by the incident wave.

For the ship wake and sea surface composite scene geometric model shown in Figure 2, the RFSFM method was used to calculate the spatially distributed backscattered field amplitude, as shown in

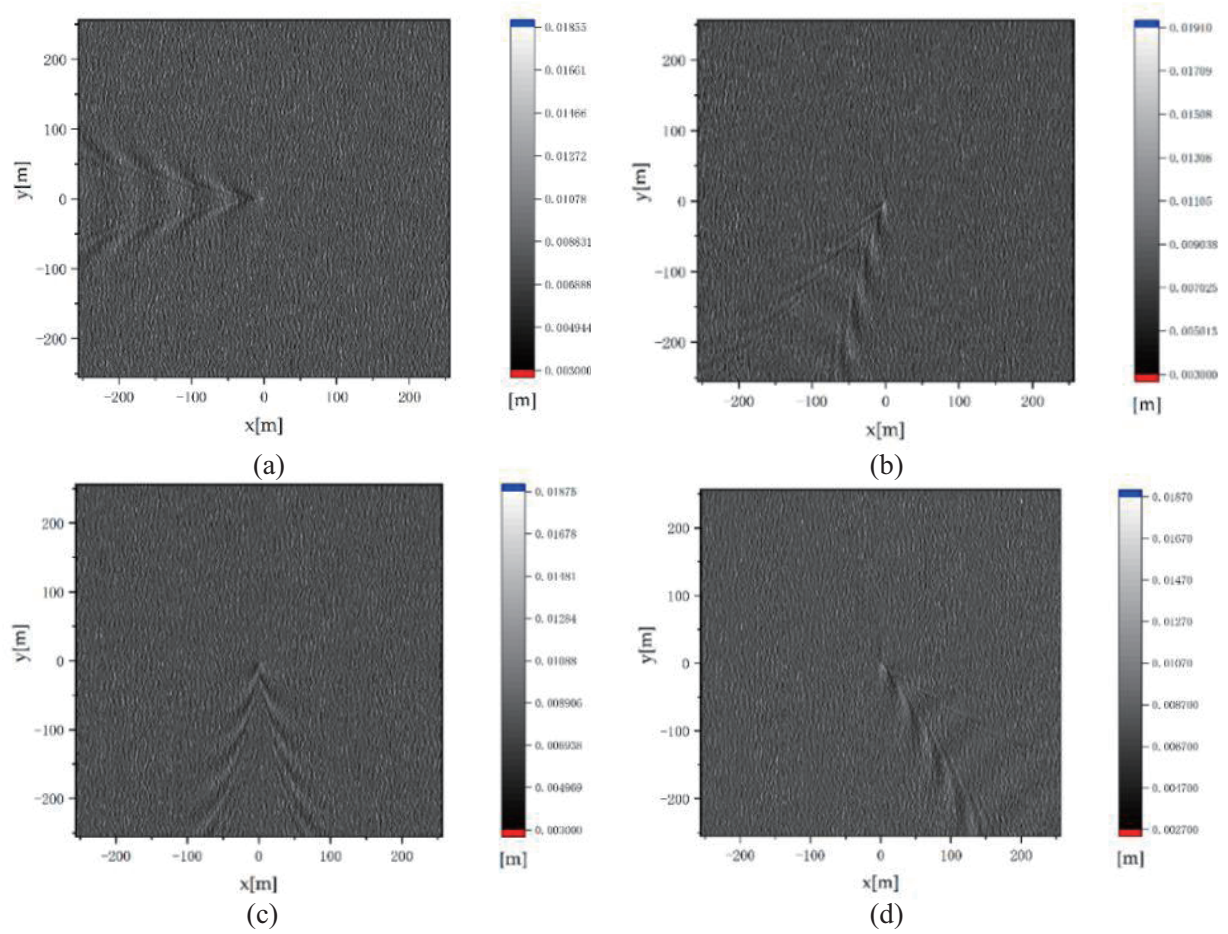

Figure 3. Spatial distribution of the scattered field amplitude of the Kelvin wake composite scene of sea surface and ship under different heading. (a) $\varphi_{ship} = 0°$, (b) $\varphi_{ship} = 45°$, (c) $\varphi_{ship} = 90°$, (d) $\varphi_{ship} = 135°$.

Figure 3, where the radar polarization mode is HH polarization; the incident wave frequency is 5 GHz; the incident angle is 50°; and the radar bearing angle is 0°. From the simulation results, it can be seen that the spatial distribution of the scattered field exhibits consistent wave texture characteristics with the original geometric model.

From the simulation results, it can be seen that when the ship motion direction is 0°, both the transverse and divergent waves in the Kelvin wake can be clearly reflected in the spatial distribution of the scattered field. When the ship's motion angle is 90°, only the scattered field distribution of divergent waves is more obvious, and when the angle is 45° or 135°, although the scattered field of divergent waves and transverse waves can be observed, only one Kelvin arm is clearer.

3.2. Scattering Calculation of Target

The GO-PO approach is a validated and effective technique for computing the electromagnetic scattering of target with multiple scattering effects [23, 24]. In accordance with this method, the target's scattering field can be represented as

$$\mathbf{E}_{pq}^{target}\left(\hat{\mathbf{k}}_i, \hat{\mathbf{k}}_s\right) = \sum_{n=1}^{N^t} \frac{\exp\left(jkR\right)}{4\pi R}\left[\hat{\mathbf{q}} \cdot \hat{\mathbf{k}}_s \times \left(\mathbf{M}_n - \eta \hat{\mathbf{k}}_s \times \mathbf{J}_n\right)\right] \cdot I_n \tag{10}$$

where η is the impedance of the free space, N^t the number of elements on the target surface, $\hat{\mathbf{q}}$ the unit polarization vector of scattered wave, and $\mathbf{M}_n, \mathbf{J}_n$ are electromagnetic flows on plane n. The Gordon method [25] enables the conversion of polygon integration over the nth patch $I_n = jk \int \exp\left[jk\left(\hat{\mathbf{k}}_i - \hat{\mathbf{k}}_s\right) \cdot \mathbf{r'_n}\right] ds'$ into contour integration. Figure 4 gives a comparison between the bistatic scattering of the ship model evaluated by GO-PO and the results evaluated by the method of equivalent currents (MEC). The frequency of incident wave is 5 GHz. The incident angle is $\theta_i = 80°$.

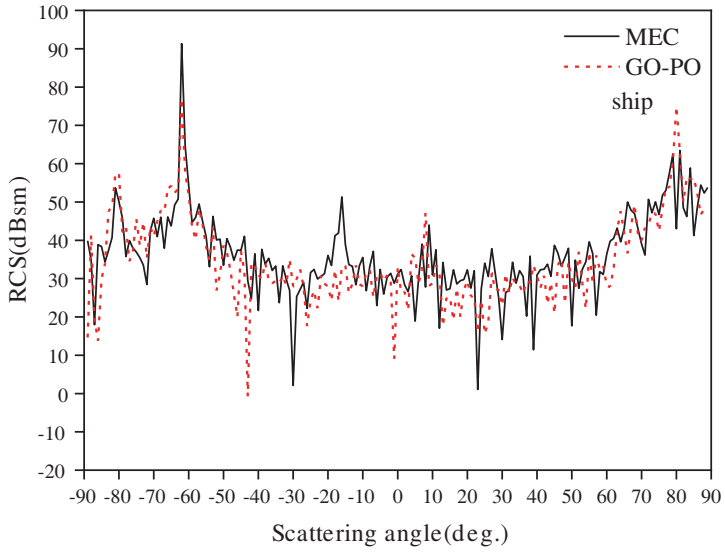

Figure 4. Validations for the scattering from ship target evaluated by GO-PO.

One can see that the results evaluated by GO-PO agree well with the result given by MEC on the whole.

3.3. Scattering Calculation of Coupled Field between Ship and Sea Surface

As shown in Figure 5, the scattering contributions of a ship in a composite scene with the sea surface mainly include the direct scattering contribution from the sea surface, the direct scattering contribution

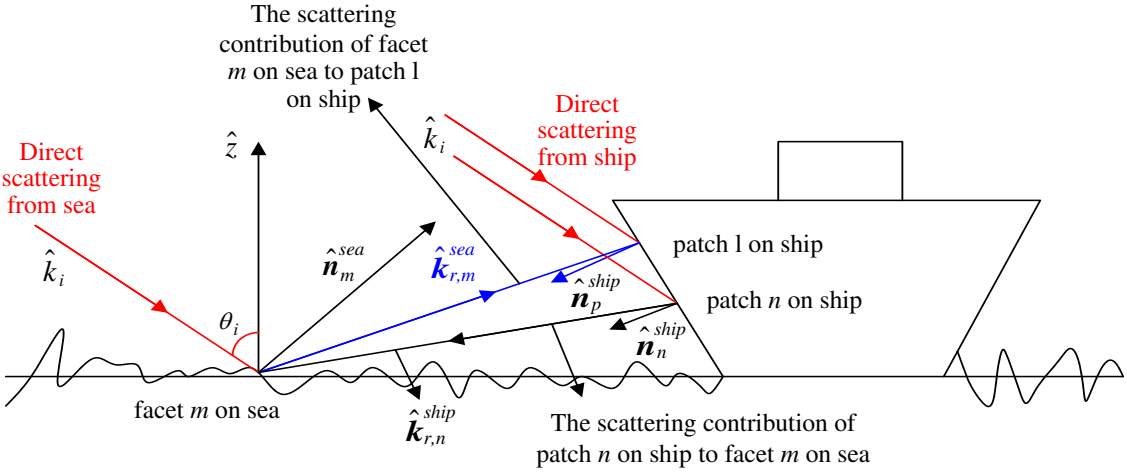

Figure 5. Diagram of the scattering contributions from composite marine scene.

from the ship, and the coupling scattering contribution between the ship and sea surface. This coupling effect includes the secondary scattering contribution of the sea surface reflected wave on the ship and the secondary scattering contribution of the ship reflected wave on the sea surface. Thus, the total field of the composite scene can be expressed as the coherent superposition of each component field:

$$\mathbf{E}^{total}\left(\hat{\mathbf{k}}_i,\ \hat{\mathbf{k}}_s\right) = \mathbf{E}^{sea}\left(\hat{\mathbf{k}}_i,\ \hat{\mathbf{k}}_s\right) + \mathbf{E}^{ship}\left(\hat{\mathbf{k}}_i,\ \hat{\mathbf{k}}_s\right) + \mathbf{E}^{cou}\left(\hat{\mathbf{k}}_i,\ \hat{\mathbf{k}}_s\right) \tag{11}$$

where,

$$\begin{aligned}\mathbf{E}^{cou}\left(\hat{\mathbf{k}}_i,\hat{\mathbf{k}}_s\right) = &\mathbf{E}^{sea->ship}\left(\hat{\mathbf{k}}_i,\hat{\mathbf{k}}_s\right) + \mathbf{E}^{ship->sea}\left(\hat{\mathbf{k}}_i,\hat{\mathbf{k}}_s\right)\\ &\frac{\exp\left(jkR\right)}{4\pi R}\sum_{m=1}^{N^s}\left[\hat{\mathbf{q}}\cdot\hat{\mathbf{k}}_s\times\left(\sum_{n=1}^{N^t} I^t_{vis,n}\cdot\mathbf{M}^s_{c,mn}\cdot I^{st}_{vis,mn} - \eta\hat{\mathbf{k}}_s\times\sum_{n=1}^{N^t} I^t_{vis,n}\cdot\mathbf{J}^s_{c,mn}\cdot I^{st}_{vis,mn}\right)\right]\cdot I_n\\ &+\frac{\exp\left(jkR\right)}{4\pi R}\sum_{l=1}^{N^t}\hat{\mathbf{q}}\cdot\hat{\mathbf{k}}_s\times\left(-\eta\hat{\mathbf{k}}_s\times\sum_{m=1}^{N^s} I^s_{vis,m}\cdot\mathbf{J}^t_{c,lm}\cdot I^{ts}_{vis,lm}\right)\cdot I_n\end{aligned} \tag{12}$$

here, $I^{st}_{vis,mn}$ is the visibility factor of sea surface element m to ship element n, and $I^{ts}_{vis,lm}$ is the visibility factor of ship element l to sea surface element m. N^s is the number of elements on the sea surface.

Finally, the total field radar cross-section (RCS) of the ship and sea surface composite model can be expressed as

$$\sigma = \lim_{R\to\infty} 4\pi R^2 \frac{\left|\mathbf{E}^{total}\right|^2}{\left|\mathbf{E}_i\right|^2} \tag{13}$$

Figure 6 compares the coupling scattering results between a rough sea surface and a ship target, evaluated using GO-PO, with the coupling scattering results obtained using the weighted four path model (WFPM). The sea surface area is 256 m × 256 m, and the grid has the size of 1.0 m × 1.0 m. The frequency of incident wave is 5 GHz. The incident angle is $\theta_i = 80°$, and wind speed is $u = 5$ m/s. One can see that the RCS from the coupling field evaluated by GO-PO is slightly lower than the result given by WFPM, but they follow the same trends. The reason for such a situation may be that in the four-path model, the rough surface below the target is regarded as a simple plane, while in the GO-PO method, the rough surface is regarded as many inclined surfaces with different normal directions. The reflection from plane is stronger than that from inclined plane. The non-negligible roughness of sea

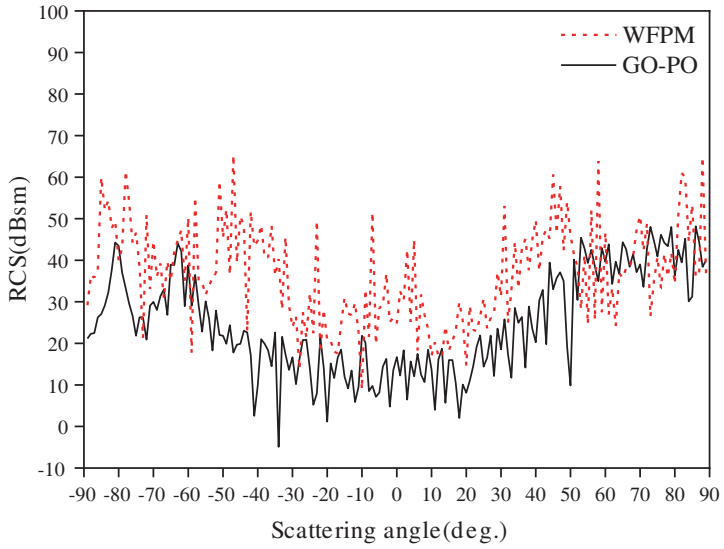

Figure 6. Verification of the GO-PO method for coupling scattering between rough sea surface and ship target.

surface is considered in GO-PO method, and the GO-PO method is more suitable to deal with the coupling scattering from target on a rough surface from the scattering mechanism point of view.

4. NUMERICAL RESULTS

This section analyzes the bistatic RCS of a composite scenario consisting of a ship on the sea surface and its wake induced, under various conditions. The incident frequency is 5 GHz; the sea surface area is 512 m × 512 m; the grid has the size of 1.0 m × 1.0 m.

The geometric model of the ship target is obtained with the help of geometric modeling software and placed in the sea surface wake scene to obtain a scene containing the sea surface, ship target, and ship wake. The composite scene composed of the destroyer and its wake generated by its movement is shown in Figure 7.

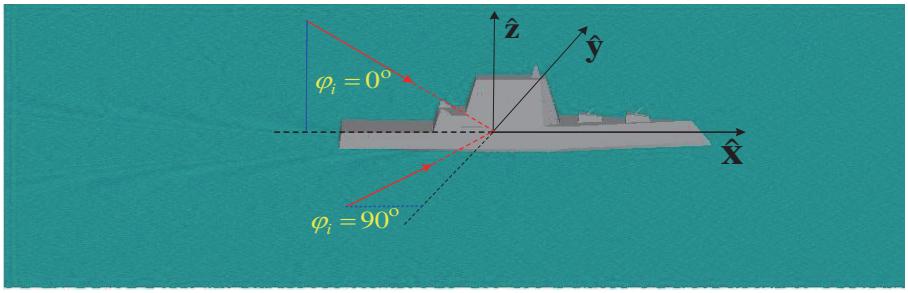

Figure 7. The schematic diagram of the composite scene of the ship target and the wake induced by the ship on the sea surface and on it.

Figure 8 presents a comparison of the total scattering coefficient, sea surface and ship wake scattering coefficient, and coupling scattering coefficient of composite scene at different incident angles under bistatic scattering conditions when the polarization mode is HH polarization, ship heading $\varphi_{sihp} = 0°$, wind speed $u = 5$ m/s, and ship speed $U_s = 10$ m/s.

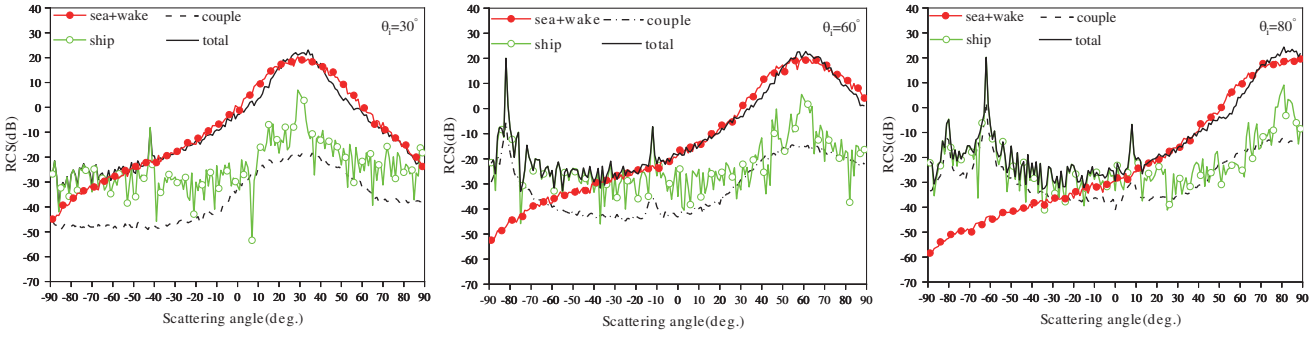

Figure 8. Bistatic scattering coefficient under different incident angles.

It can be observed that when the incidence angle is 30 degrees, both in the mirror scattering region and backscattering region, the scattering contribution from the sea surface and ship wake dominates. When the incidence angle reaches 60 degrees, in the mirror scattering region, the scattering contributions from the sea surface and ship wake dominate, while in the backscattering region, the contributions from ship and coupling scattering increase. When the incidence angle reaches 80 degrees, the contributions from ship and coupling scattering dominate in the backscattering region, but in the mirror scattering region, the scattering contribution from the sea surface and ship wakes still dominates.

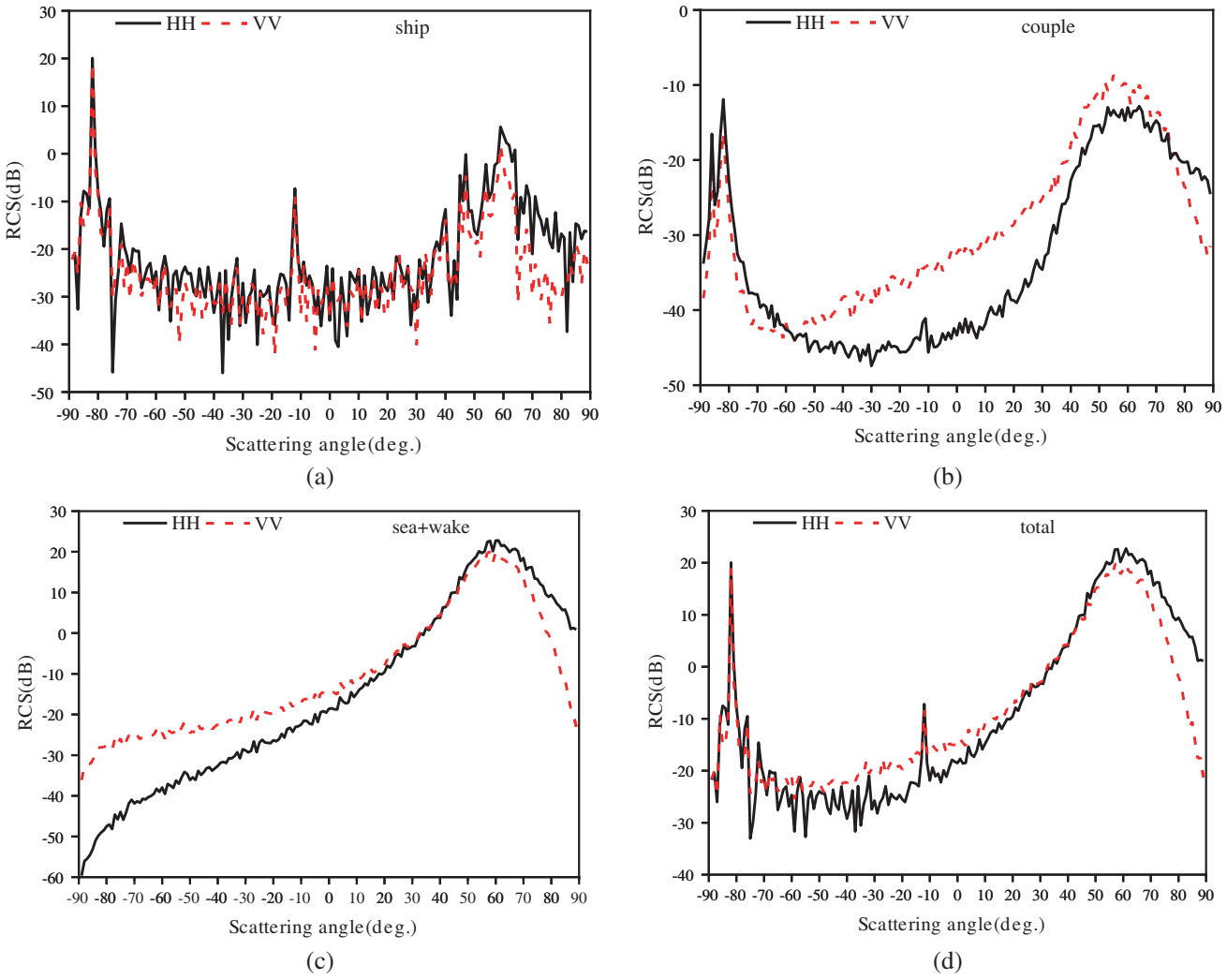

Figure 9. Bistatic scattering coefficient under different polarization modes.

Figure 9 presents a comparison of the total scattering coefficient, sea surface and ship wake scattering coefficient, and coupling scattering coefficient of composite scene at different polarization modes under bistatic scattering conditions when the incidence angle $\theta_i = 60°$, ship heading $\varphi_{sihp} = 0°$, wind speed $u = 5\,\mathrm{m/s}$, and ship speed $U_s = 10\,\mathrm{m/s}$.

It can be observed from the figure that the RCS of ship target under HH polarization is larger than that under VV polarization in the whole scattering interval. When the scattering angle is less than -60 degrees and the scattering angle greater than 70 degrees, the coupling scattering under HH polarization is greater than that under VV polarization. On the contrary, the coupling scattering contribution under VV polarization is much greater than that under HH polarization in the range from -60 degrees to 70 degrees. When the scattering angle is less than 30 degrees, the composite scattering RCS of sea surface and wake under VV polarization is greater than that under HH polarization, whereas when the scattering angle is greater than 30 degrees, the composite scattering RCS of sea surface and wake under HH polarization will be greater than that under VV polarization. This is also the reason that the variation law of total radar scattering coefficient of the whole composite scene is similar to that of coupling scattering.

Figure 10 shows the total bistatic scattering coefficient of the composite scene at different incidence angles, with HH polarization, ship heading $\varphi_{sihp} = 0°$, wind speed $u = 3\,\mathrm{m/s}$, and ship speed $U_s = 10\,\mathrm{m/s}$.

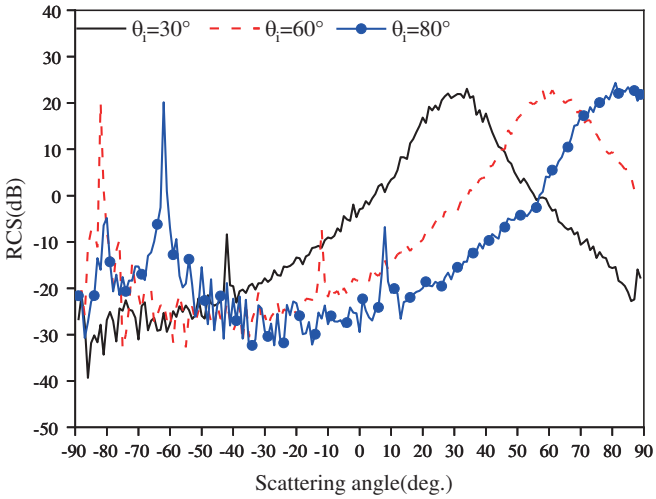

Figure 10. The total bistatic scattering coefficient of the composite scene at different incidence angles.

From the figure, it can be seen that more ship scattering information can be obtained when the incidence angle increases to 80 degrees. When the incidence angle is 80 degrees, two peaks appear in the scattering angle range of −90 to −50 degrees, which are caused by the scattering from the two turrets on the ship. When the incidence angle is small, only one peak is observed in this range because the radar can only receive the scattering signal from one of the turrets at a small incidence angle.

Figure 11 shows the comparison of the bistatic scattering coefficients of a ship on a sea surface with and without wake, with HH polarization heading of 0 degrees, incidence angle $\theta_i = 80°$, wind speed $u = 3\,\mathrm{m/s}$, and ship speed $U_s = 10\,\mathrm{m/s}$.

From Figure 11(a) it can be seen that the presence of wake leads to a lower bistatic scattering coefficient of the sea surface in the backscattering region than in the pure sea surface, while in the mirror scattering region, the presence of wake leads to a higher bistatic scattering coefficient of the sea surface than in the pure sea surface. This reflects that the presence of the wake changes the roughness of the sea surface. This is also the reason that in Figure 11(b) the bistatic scattering coefficient of a ship on pure sea surface is greater than that of a ship on a sea surface with wake.

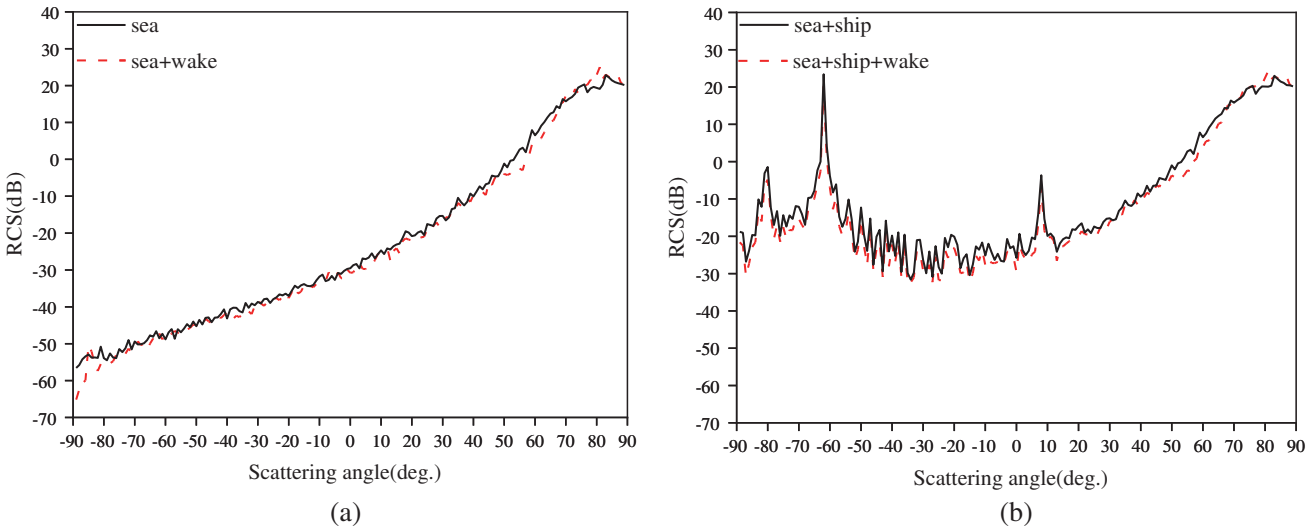

Figure 11. The comparison of the bistatic scattering coefficients of a ship on a sea surface with and without wake.

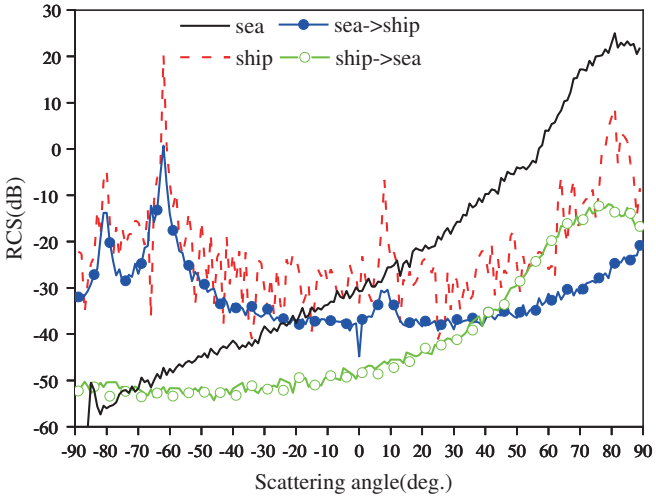

Figure 12. The comparison of the ship's own scattering contribution and the scattering contribution from the sea surface to the ship and from the ship to the sea surface.

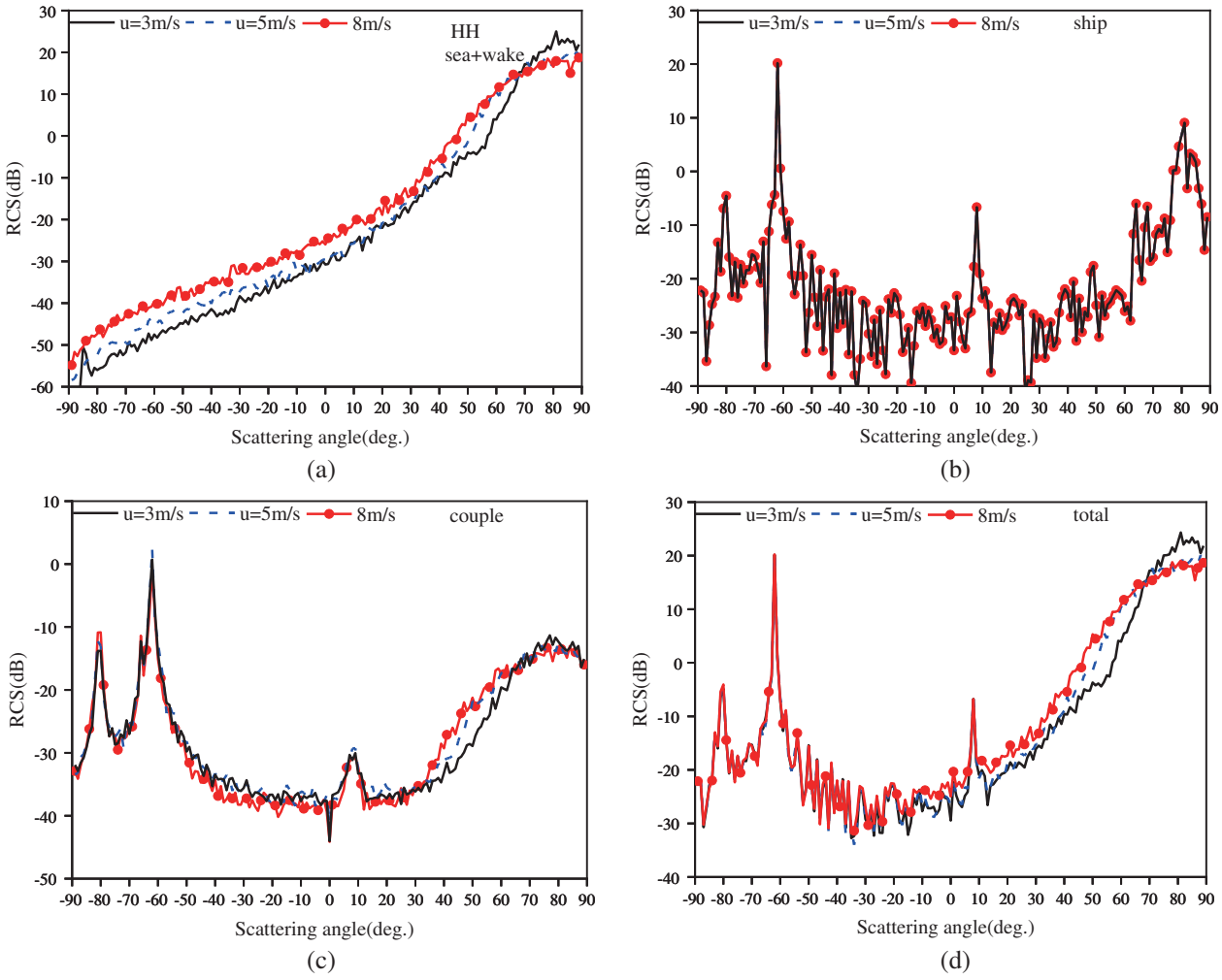

Figure 13. Bistatic scattering RCS under different wind speeds.

Figure 12 shows the comparison of the ship's own scattering contribution and the scattering contribution from the sea surface to the ship and from the ship to the sea surface, with HH polarization, incidence angle $\theta_i = 80°$, wind speed $u = 3\,\mathrm{m/s}$, ship speed $U_s = 10\,\mathrm{m/s}$, and ship heading $\varphi_{sihp} = 0°$. It can be observed that the scattering contributions of the ship itself and the sea surface to the ship under HH polarization dominate, and after entering the mirror scattering area, their scattering contributions will be overwhelmed by the scattering contributions of the sea surface. Throughout the scattering area, the ship's scattering contribution to the sea surface is relatively weak.

Figure 13 depicts the ship RCS, sea surface RCS, and coupling scattering RCS and total RCS under different wind speeds when the polarization mode is HH polarization, heading $\varphi_{sihp} = 0°$, incidence angle $\theta_i = 80°$, and ship speed $U_s = 10\,\mathrm{m/s}$.

It can be observed from the figure that the radar scattering coefficient of the sea surface with ship wake increases with the increase of wind speed before the specular scattering area, but it does decrease with the increase of wind speed in the specular scattering area. This is due to the increase of wind speed, which increases the roughness of the sea surface and enhances the diffuse reflection of the sea surface. The increase of wind speed will not affect the radar scattering coefficient of ship targets. In the backscattering area, the diffuse reflection of the sea surface increases due to the increase of wind speed, which makes the coupling radar scattering coefficient between the ship and the sea surface decrease with the increase of wind speed. This also leads to the decrease of the total radar scattering coefficient

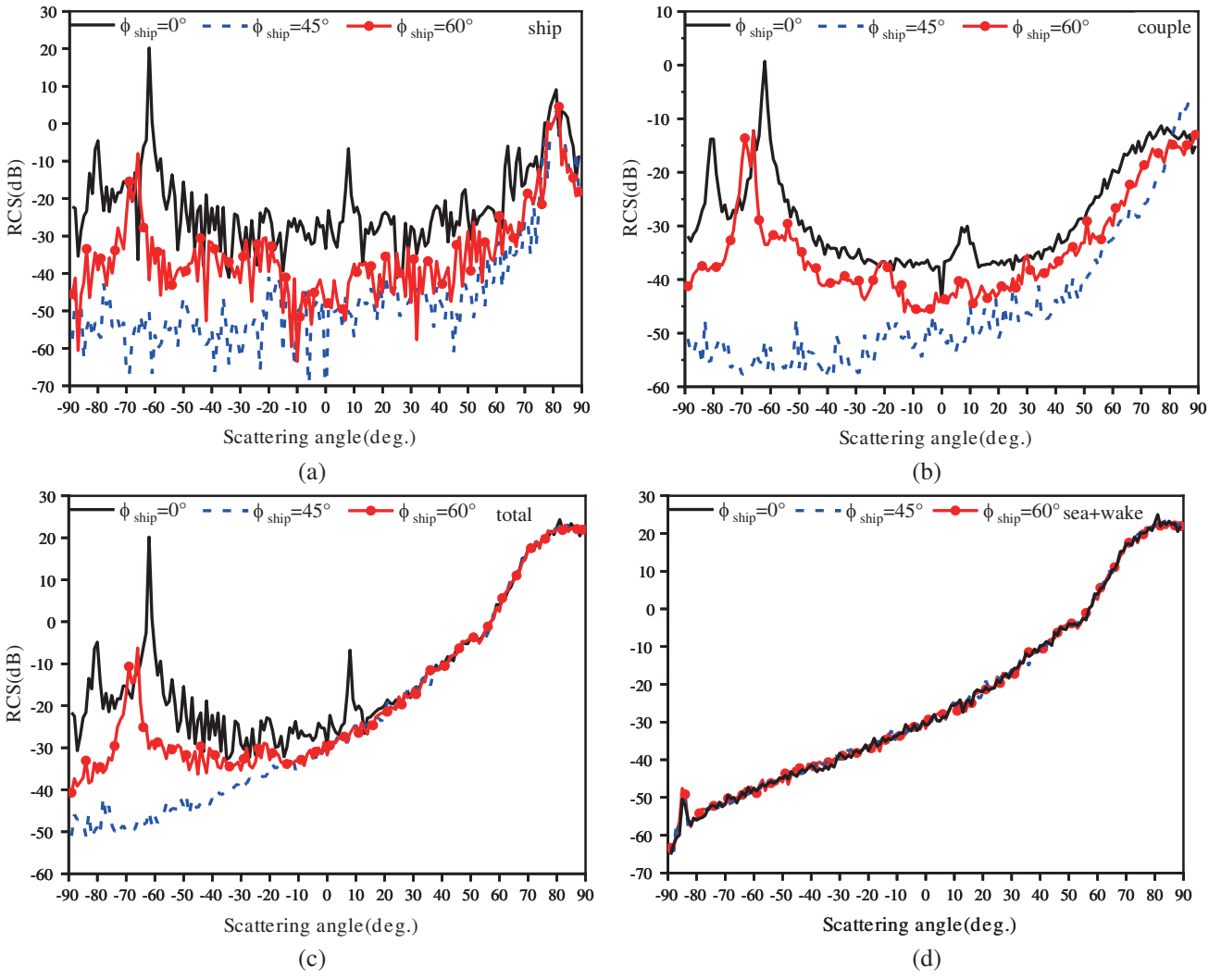

Figure 14. The bistatic scattering coefficient at different ship headings.

of the whole composite scene in the backscattering area with the increase of wind speed.

Figure 14 shows the bistatic scattering coefficient at different ship headings with HH polarization, ship speed $U_s = 10\,\mathrm{m/s}$, wind speed $u = 3\,\mathrm{m/s}$, and incidence angle $\theta_i = 80°$.

It can be observed from the figure that due to the change of course, the RCS of the ship, the RCS of the sea surface, the RCS of coupling scattering, and the total RCS of the whole composite scene have changed to varying degrees. With the change of course, the change of RCS of the sea surface is relatively small compared with that of the ship. At the same time, it can be observed that the RCS of bistatic scattering is the largest in backscattering, because radar can receive more scattering information in backscattering.

5. CONCLUSIONS

In this paper, the electromagnetic scattering characteristics of the composite scenes of sea surface, ship target, and wake induced by ship are studied. After establishing the composite scenes of surface, ship target, and wake trails, the composite electromagnetic scattering coefficients under different conditions are calculated by combining RFSFM and GO-PO methods. The results show that the radar can receive more ship scattering echoes at a large incidence angle and an angle of 0° between the radar's apparent direction and the ship's motion direction. The next study will focus on the electromagnetic scattering from a moving ship with time-varying ship wake over a time-varying sea surface.

DISCLOSURE STATEMENT

No potential conflict of interest was reported by the authors.

ACKNOWLEDGMENT

This work was supported in part by the National Natural Science Foundation of China (Grant Nos. 62261054 and 62061048), in part by Shaanxi Provincial Science and Technology Department (No. 2023-YBGY-254) and in part by Yan'an University Postgraduate Education Innovation Project (YCX202323).

REFERENCES

1. Yao, C., C. Li, X. Jin, and L. Zhang, "A fast two-parameter CFAR algorithm based on FFT for ship detection in large-scale SAR images," *2022 5th International Conference on Information Communication and Signal Processing (ICICSP)*, 244–248, Shenzhen, China, November 26–28, 2022.
2. Bai, L., C. Yao, Z. Ye, D. Xue, X. Lin, and M. Hui, "A novel anchor-free detector using global context-guide feature balance pyramid and united attention for SAR ship detection," *IEEE Geoscience and Remote Sensing Letters*, Vol. 20, 1–5, 2023.
3. Qian, G., Y. Wang, and M. Jian, "Estimation of doppler parameters based on PSO for BFSAR ship target imaging," *IEEE Geoscience and Remote Sensing Letters*, Vol. 20, 1–5, 2023.
4. Wang, Z., Y. Li, Y. Li, J. Zhao, Y. Huang, and S. Shao, "Research on compound scattering modeling and imaging methods of sea surface ship target for GEO-UAV BiSAR," *2022 3rd China International SAR Symposium (CISS)*, 1–5, Shanghai, China, November 2–4, 2022.
5. Zhang, Y., M. Xing, J. Zhang, G.-C. Sun, and D. Xu, "Robust multi-ship tracker in SAR imagery by fusing feature matching and modified KCF," *IEEE Geoscience and Remote Sensing Letters*, Vol. 20, 1–5, 2023.
6. Li, N., X. Pan, L. Yang, Z. Huang, Z. Wu, and X. Zhang, "Ship target detection method based on local saliency enhancement," *2022 IEEE 5th International Conference on Electronic Information and Communication Technology (ICEICT)*, 619–623, Hefei, China, August 21–23, 2022.

7. Wu, P., S. J. Su, X. Z. Tong, R. Guo, B. Sun, and J. J. Zahng, "SARFB: Strengthened asymmetric receptive field block for accurate infrared ship detection," *IEEE Sens. J.*, Vol. 23, 5028–5044, 2023.
8. Huang, Y., Z. Zhao, Z. Nie, and Q.-H. Liu, "Dynamic volume equivalent SBR method for electromagnetic scattering of targets moving on the sea," *IEEE Trans. Antennas Propag.*, Vol. 20, 3509–3519, 2023.
9. Shi, F., J. Li, W. Jiang, M. Zhang, and Z. Li, "Research on scattering characteristics of ship targets on two-dimensional dynamic sea surface," *2021 Cross Strait Radio Science and Wireless Technology Conference (CSRSWTC)*, 180–182, Shenzhen, China, October 11–13, 2021.
10. Luo, G., Z. H. Xiong, M. B. Zhou, Q. X. Wan, and Z. Ren, "A study of electromagnetic scattering from kelvin ship wake on the finite depth sea surface," *2022 International Conference on Microwave and Millimeter Wave Technology (ICMMT)*, 1–3, Har-bin, China, August 12–15, 2022.
11. Sun, X. F., M. Y. Cai J. K. Wang, and C. L. Liu, "Numerical simulation of the Kelvin wake patterns," *Appl. Sci.*, Vol. 12, 6265, 2022.
12. Wang, H., D. Nie, Y. Zuo, L. Tang, and M. Zhang, "Nonlinear ship wake detection in SAR images based on electromagnetic scattering model and YOLOv$_5$," *Remote Sens.*, Vol. 14, 5788, 2022.
13. Song, M. Z., R. Guo, X. R. Ma, Y. T. Chen, and J. S. Wang, "Polarization reflection distribution characteristics of wakes on the sea surface," *Appl. Opt.*, Vol. 61, 7748–7756, 2022.
14. Li, J., L. Wang, M. Zhang, Y. -C. Jiao, and G. Liu, "Ship velocity automatic estimation method via two-dimensional spectrum pattern of kelvin wakes in SAR images," *IEEE J. Sel. Top Appl. Earth Obs. Remote Sens.*, Vol. 14, 4779–4786, 2021.
15. Bi, N., J. Qin, and T. Jiang, "Partition detection and location of a kelvin wake on a 2-D rough sea surface by feature selective validation," *IEEE Access*, Vol. 6, 16345–16352, 2018.
16. Deng, Y., M. Zhang, and L. Wang, "SAR image simulation analysis of sea surface containing underwater object wake," *2019 6th Asia-Pacific Conference on Synthetic Aperture Radar (APSAR)*, 1–4, Xiamen, China, November 26–29, 2019.
17. Wei, Y., Z. Wu, H. Li, J. Wu, and T. Qu, "Application of periodic structure scattering in kelvin ship wakes detection," *Sustain. Cities Soc.*, Vol. 47, Art. No. 101463, May 2019.
18. Elfouhaily, T., B. Chapron, K. Katsaros, and D. Vandemark, "A unified directional spectrum for long and short wind-driven waves," *J. Geophys. Res.*, Vol. 102, 15781–15796, 1997.
19. Wang, L., L. Guo, and X. Meng, "Research on electromagnetic scattering characteristics of kelvin wake of ship based on MPI," *2018 12th International Symposium on Antennas, Propagation and EM Theory (ISAPE)*, 1–4, Hangzhou, China, December 3–6, 2018.
20. Zhang, M., H. Chen, and H. Yin, "Facet-based investigation on EM scattering from electrically large sea surface with two-scale profiles: Theoretical model," *IEEE Trans. Geosci. Electron.*, Vol. 49, 1967–1975, 2011.
21. Zhao, Y., X. Yuan, M. Zhang, and H. Chen, "Radar scattering from the composite ship-ocean scene: Facet-based asymptotical model and specular reflection weighted model," *IEEE Trans. Antennas Propag.*, Vol. 62, 4810–4815, 2014.
22. Xu, F. and Y. Jin, "Bidirectional analytic ray tracing for fast computation of composite scattering from electric-large target over a randomly rough surface," *IEEE Trans. Antennas Propag.*, Vol. 57, 1495–1505, 2009.
23. Zhang, M., Y. Zhao, J. X. Li, and P.-B. Wei, "Reliable approach for composite scattering calculation from ship over a sea surface based on FBAM and GO-PO models," *IEEE Trans. Antennas Propag.*, Vol. 65, 775–784, 2017.
24. Wei, P. B., M. Zhang, W. Niu, and W. Q. Jiang, "GPU-based combination of GO and PO for electromagnetic scattering of satellite," *IEEE Trans. Antennas Propag.*, Vol. 60, 5278–5285, 2012.
25. Gordon, W., "Far-field approximations to the Kirchhoff-Helmholtz representations of scattered fields," *IEEE Trans. Antennas Propag.*, Vol. 23, 590–592, 1975.